14th International Symposium on Turbulence and Shear Flow Phenomena (TSFP14)
Heidelberg, Germany, July 28–31, 2026

WEAKLY NONLINEAR OPTIMAL PERTURBATION ANALYSIS FOR SHEAR FLOW

Nobutaka Taniguchi
Institute of Fluid Science
Tohoku University
2-1-1 Katahira, Aoba-ku, Sendai, Miyagi, Japan
nobutaka.taniguchi.c1@tohoku.ac.jp

Aiko Yakeno
Institute of Fluid Science
Tohoku University
2-1-1 Katahira, Aoba-ku, Sendai, Miyagi, Japan
aiko.yakeno@tohoku.ac.jp

ABSTRACT

The accurate tracking of mean flow distortion and double-harmonic wave evolution is critical to elucidate laminar-to-turbulent transition. When the initial disturbance field consists of a limited number of discrete normal modes, perturbation expansion enables the prediction of possible nonlinear interactions. The idea of weakly nonlinear optimal perturbation (WNLOP) was first proposed by Pralits et al. (J. Fluid Mechanics, 2015), where the regular perturbation expansion was applied in incompressible flows. This study presents a reformulation by using the coupled amplitude equations to incorporate the effect of double-harmonic waves in the evolution of disturbance field for compressible flows. The theoretical prediction and its limitation are discussed in detail, where we solved the plane Poiseuille flow in nearly incompressible condition as a benchmark problem to discuss its properties. From this study, we confirmed that the prediction by the present WNLOP formulation shows a high accuracy in a comparison with implicit large-eddy simulations (ILES), while it also produces spurious second peak originating from specific combination of eigenmodes as a limitation of current framework.

Introduction

Non-modal stability analysis provides a fundamental understanding of the transient disturbance growth over a finite time. The concept was developed to bridge the gap between the stability criteria derived from the linear stability theory and the criteria obtained from experiments and energy method (Reddy & Henningson (1993)). The amplification of small disturbances is attributed to the non-normal nature, especially for shear flows, of the linearized Navier–Stokes (N–S) equations (Trefethen *et al.* (1993)). In this analysis, optimal perturbations, which are initial disturbances that yield the largest possible growth over a given time, provide crucial insights into the path of laminar-to-turbulent transition including the lift-up mechanism of streamwise vortices (Trefethen *et al.* (1993); Reddy & Henningson (1993)).

The role of nonlinearity in the growth of finite-amplitude disturbances has been extensively studied for decades. In pioneering studies, the nonlinear evolution of linear optimal perturbations (LOP) has been analyzed for shear flows by Butler & Farrell (1994) and for simple models by Trefethen *et al.* (1993). They demonstrated that the finite disturbance field, after being enhanced by the linear amplification mechanisms, was trapped in a finite-amplitude attractor of the system. Pringle & Kerswell (2010); Cherubini *et al.* (2010) formulated methods for determining finite-amplitude optimal perturbations, which enabled the direct consideration of nonlinear effects in their calculation. In a review article, Kerswell (2018) classified optimal perturbations based on the degree of nonlinear effects in quasi-linear optimal perturbations (QLOPs) and nonlinear optimal perturbations (NLOPs). They noted that nonlinearity initially suppresses linear amplification while preserving the qualitative structure of LOPs in a case of QLOP. However, after a certain critical value of the initial disturbance magnitude, the evolution changes into a qualitatively different path, characteristic of an NLOP. For incompressible boundary layer flow, Cherubini *et al.* (2010) reported that NLOPs showed spatial modulation and localization, and they demonstrated that these distributional changes led to transition. Numerous studies have been conducted to reveal the characteristics of transition using the approach of nonlinear non-modal analysis.

However, the high computational cost associated with determining NLOPs hampers the application of these approaches to laminar-to-turbulent transition process. In this context, weakly nonlinear theory has long been studied to model the key nonlinear effects on disturbance growth (§26 in Landau & Lifshitz (2013) and §49 in Drazin & Reid (2004)). In non-modal analysis, Pralits *et al.* (2015) proposed a weakly nonlinear optimal perturbation (WNLOP) analysis that accounts for the nonlinear interaction between the disturbance field and the mean-flow distortion. Their analysis aims to model the mean flow distortion by the Reynolds stress of the disturbance field. More recently, Ducimetière & Gallaire (2025) derived a set of nonlinear amplitude equations to incorporate the weakly nonlinear effects into the time evolution of the disturbance field. In the context of resolvent analysis, Rigas *et al.* (2021) formulated a method that incorporates nonlinear interaction between multiple discrete wavenumbers within the harmonic balanced N–S equations. These approaches significantly reduce the computational cost of predicting nonlinear effects.

This study aims to extend the approach of Pralits *et al.* (2015) to WNLOP with a consideration of double-harmonic waves and mean flow distortion in compressible N–S equations, using a framework of coupled amplitude equations. The primary theoretical advance of the present analysis is the definition of WNLOP within a space spanned by the eigenmodes of linear stability theory (LST), representing a natural extension of the classic theory of linear optimal perturbations.

Governing equation

In this study, we consider the plane-Poiseuille (pPF) flow between the two plates located at $z = \pm h$. The streamwise, spanwise, and wall-normal coordinates are denoted by x, y, and z, respectively. The flow between these plates is driven by a constant pressure gradient, $2dP_0/dx$. The flow variables are non-dimensionalized using the centerline density, the mean wall temperature of the two plates, channel half-width h, and the pressure gradient between the plates. The governing equations are the non-dimensional compressible N–S equations as

$$\partial_t \rho + u_j \partial_j \rho = -\rho \partial_j u_j, \tag{1}$$

$$\rho \partial_t u_i + \rho u_j \partial_j u_i = -\frac{1}{\gamma M^2} \partial_i (\rho T) + \partial_j \tau_{ij}, \tag{2}$$

$$\rho \partial_t T + \rho u_j \partial_j T = -\tilde{\gamma} \rho T \partial_j u_j + A \partial_j (\kappa \partial_j T) + B \partial_j u_i \tau_{ij}, \tag{3}$$

where $\rho, u_i, p, T, \gamma (= \tilde{\gamma} + 1)$ are the density, velocity, pressure, temperature, and the specific heat ratio. The parameters A and B are defined as $A = \gamma/(PrRe), B = \gamma\tilde{\gamma}M^2$, respectively. The viscous stress tensor is expressed as

$$\tau_{ij} = \frac{\mu}{Re} \left(\partial_j u_i + \partial_i u_j - \frac{2}{3} \delta_{ij} \partial_k u_k \right), \tag{4}$$

under Stokes' hypothesis for the bulk viscosity where μ, κ are the coefficient of viscosity and thermal conductivity. In this formulation, the non-dimensional parameters of Reynolds number Re, Prandtl number Pr, and Mach number M are introduced based on the reference values above.

The reduction to the one-dimensional equations is required to obtain the base flow field. Under the parallel-flow assumption, these equations simplify to

$$\frac{2}{Re} + \mu_0 \frac{d^2 U_0}{dz^2} + \left(\frac{d\mu}{dT} \right)_0 \frac{dT_0}{dz} \frac{dU_0}{dz} = 0, \tag{5}$$

$$\frac{\mu_0}{Pr} \frac{d^2 T_0}{dz^2} + \frac{1}{Pr} \left(\frac{d\mu}{dT} \right)_0 \left(\frac{dT_0}{dz} \right)^2 + \mu_0 \tilde{\gamma} M^2 \left(\frac{dU_0}{dz} \right)^2 = 0, \tag{6}$$

where $\bar{q} = (\rho_0, U_0, 0, 0, T_0)^T$ is the base flow. Assuming that the wall-temperatures of two plates are equal, boundary conditions at both walls are prescribed as

$$T_0 = 1, U_0 = 0, \tag{7}$$

at $z = \pm 1$. In the incompressible limit, this base flow naturally reduces to the well-known pPF for incompressible flow as $U_0 = 1 - z^2, T_0 = 1$.

Formulation of weakly nonlinear equations

We introduce the state vector $q = (\rho, m_x, m_y, m_z, p)^T$ and we consider the flow decomposition into base flow $\bar{q}$ and the perturbation q' as $q = \bar{q} + q'$. When the base flow field is a solution of steady compressible N–S equation, the nonlinear perturbation can be expressed as

$$\partial_t q' + L(\bar{q}) q' = N(q', q') + O(|q'|^3) \tag{8}$$

where we consider the perturbation up to the second order. Here, L and N denote the linearized N–S operator and the nonlinear term, respectively. We also introduce $\{\sigma_j\}_j$ as the eigenvalues of L for the further discussions. In the case of compressible flow field, the third-order expansions of nonlinear terms is also required to incorporate the effect of density fluctuation rigorously, while fourth and higher-order expansions require the strict incorporations of temperature fluctuations. Mathematically, since we consider the nonlinear feedback up to the third-order, the expansion also requires the third-order for the strict discussion. However, since this study focuses on the nonlinear effect of double-harmonic waves in low subsonic flow regime, we neglect these terms. Here, $N(q', q')$ represents the nonlinear term, where $N(f, g) = N(g, f)$ for any vectors f, g is defined such that it satisfies commutativity of N.

Following the discussion of amplitude equation (Fujimura (1989)), we expand the perturbations q' into $q' = q_1 + q_2 + q_3$ as

$$q_1 = \sum_j \psi_{11}^j (z) A_j \mathrm{e}^{i\boldsymbol{k}\cdot\boldsymbol{x}} + \sum_j \psi_{13}^{jkl} (z) A_j A_k A_l^* \mathrm{e}^{i\boldsymbol{k}\cdot\boldsymbol{x}} + \text{c.c.} + \dots, \tag{9}$$

$$q_2 = \sum_{jk} \psi_{22}^{jk} (z) A_j A_k \mathrm{e}^{2i\boldsymbol{k}\cdot\boldsymbol{x}} + \text{c.c.} + \dots, \tag{10}$$

$$q_3 = \sum_{jk} \psi_{02}^{jk} (z) A_j A_k^* + \dots. \tag{11}$$

Here, the superscript asterisk and c.c. denote the complex conjugates and $\psi_{11}^j, \psi_{13}^{jkl}, \psi_{22}^{jk}, \psi_{02}^{jk}$ represent the expansion coefficients of the fundamental wave $\boldsymbol{k} = (k_x, k_y)$, the double-harmonic wave and the mean flow fistortion, respectively. To ensure that the flow field remains real-valued, it is required that

$$\psi_{11}^j = (\psi_{-11}^j)^*, \psi_{22}^{jk} = (\psi_{-22}^{jk})^*, \tag{12}$$

where $\psi_{-11}^j, \psi_{-22}^{jk}$ are the coefficients for $-\boldsymbol{k}, -2\boldsymbol{k}$, respectively. Here, A_j represents the amplitude of j-th mode of the fundamental wave. Following Watson (1960), we assume that the form of Landau equation as

$$\frac{dA_j}{dt} = \sigma_j A_j + \sum_{klm} \Lambda_{jklm} A_k A_l A_m^* \tag{13}$$

where σ_j is the j-th eigenvalue and Λ_{jklm} denotes the Landau coefficient. By following the standard procedure, we obtain

$$\sigma_j \psi_{11}^j + \hat{L}_k \psi_{11}^j = 0, \tag{14}$$

$$\{(\sigma_j + \sigma_k) I + \hat{L}_{2k}\} \psi_{22}^{jk} = N(\psi_{11}^j, \psi_{11}^k), \tag{15}$$

$$\{(\sigma_j+\sigma_k^*)I+\hat{L}_0\}\psi_{02}^{jk}=N(\psi_{11}^j,\psi_{-1,1}^k)+N(\psi_{-11}^j,\psi_{11}^k), \tag{16}$$

and

$$\sum_j \psi_{11}^j\Lambda_{jklm}+\{(\sigma_k+\sigma_l+\sigma_m^*)I+\hat{L}_k\}\psi_{13}^{klm}=N(\psi_{02}^{km},\psi_{11}^l)+N(\psi_{22}^{kl},\psi_{-1,1}^m) \tag{17}$$

where $\hat{L}_k,\hat{L}_{2k},\hat{L}_0$ are the linear operator for the wavenumber $k,2k,0$.

Since σ_j is an eigenvalue of $-\hat{L}_k$, we can close (17) for single mode, and ψ_{13}^{klm} can be eliminated by solvability condition. In more general cases, the amplitude at some reference point $z=z_0$ is fixed so that $\psi_{11}^j(z_0)=1,\psi_{13}^{klm}(z_0)=0$ to obtain the Landau coefficient, where its definition depends on the selection of reference point. However, it seems that this definition requires a careful selection to avoid the zeros of all the considered eigenmodes, otherwise it takes the numerically unstable values. To avoid these issues, we assume that the third-order expansion belongs to the orthogonal complement as

$$\langle\psi_{13}^{klm},(\psi_{11}^j)^\dagger\rangle=0. \tag{18}$$

where $(\psi_{11}^j)^\dagger$ is the adjoint eigenmodes of ψ_{11}^j. In this case, we can obtain the evaluation of Λ_{jklm} as

$$\Lambda_{jklm}=\langle(\psi_{11}^j)^\dagger,N(\psi_{02}^{km},\psi_{11}^l)+N(\psi_{22}^{kl},\psi_{-1,1}^m)\rangle. \tag{19}$$

To define the norm in compressible flow field, we adopt the norm proposed by (Mack (1984); Hanifi *et al.* (1996)) as

$$||q'||_e^2:=\frac{1}{2}\int_{-1}^{1}\left(\bar{\rho}|u_i|'^2+\frac{\bar{T}|\rho'|^2}{\bar{\rho}\gamma M^2}+\frac{\bar{\rho}|T'|^2}{\gamma(\gamma-1)\bar{T}M^2}\right)dz. \tag{20}$$

This definition allows for the extension of the definition of WNLOP and NLOP (Pralits *et al.* (2015); Cherubini *et al.* (2010); Pringle & Kerswell (2010)): the WNLOP solution is defined to maximize $||q_1(t=t_f)||_e^2$ subject to the constraint condition of $||q_1(t=0)||_e^2=\delta_0^2$ subject to the governing equations (13). Since we consider the asymptotic expansion up to third order, the rigorous definition of the norm should be defived from (9) while the identification of third-order feedback terms ψ_{13}^{klm} is computationally expensive to evaluate the disturbance magnitude. In spite of its mathematical rigor from the definition, this evaluation scales with $O(N^3\times K)$ where K is the dimension of the freedom of variables and grid points, rendering the computation intractable with a large number of eigenmodes N.

To circumvent these computational difficulties, we applied the approximate definition of disturbance norm as

$$||q'||_a^2=||\sum_j\psi_{11}^j(z)A_j||_e^2 \tag{21}$$

where the higher terms are regarded as corrections to the first-order terms. Because of the scale separation, this approximation can be justified by the scale separation, as the effects of nonlinear interactions up to the third-order feedback process are already incorporated into the amplitude coefficients. The validity of this approximation will be demonstrated through comparison with the numerical results by implicitly large-eddy simulations (ILES).

Because we have fixed the evaluation function in (21) and the weakly nonlinear model in (13), it is possible to formulate the WNLOP following Pralits *et al.* (2015). However, it should be considered that the weakly nonlinear model may yield a narrow optimal solution characterized by large Hessian values, based on our observation of the numerical experiments especially at the weakly nonlinear region. The alternative options relating to the stabilization techniques of optimization processes were discussed, but the current approach does not incorporate these techniques to maintain the fiedelity of the original objective function. Therefore, we introduce the following Lagrangian as

$$\mathscr{L}=||q'(t_f)||_a^2, \tag{22}$$

and the constraint condition is that the constant amplitude of initial disturbance field $||q'(t_0)||_2=\delta_0$ with a given scalar value δ_0 and the condition that the disturbance field follows (13). The Jacobian of (22) can be obtained by the numerical derivative with respect to each amplitude variables $\{A_i\}$, and the steepest ascent method on the manifold was applied in the optimization procedure.

Tensor-Train (TT) decomposition

Theoretically, the expansion in (13) requires the reduction product of third-order tensor, which prevents the progress of coupled amplitude equations. In this study, we introduce the recent achievement of TT decomposition by Oseledets (2011) to resolve this issues. In general, the TT decomposition is a method to approximate the high-order tensors by avoiding the curse of dimensionality. When we approximate the m-th order Tensors $A\in \mathrm{R}^{N\times M}$ as

$$A=\mathscr{G}_0\mathscr{G}_1\cdots\mathscr{G}_M \tag{23}$$

where $\mathscr{G}_i$ is the third-order tensors, which is called as the tensor core. Numerically, we applied the TT decomposition based on singular value decomposition (TT-SVD), whose truncation accuracy is selected to 10^{-5}. This decomposition is applied to the right-hand-side in (19) to approximate and second term of RHS in (13) directly.

Numerical methods and flow settings

In this study, we applied 6-th order compact difference method (Lele (1992)) to approximate the coefficients of differential operators in (8). This discretization method is commonly used to obtain the direct and adjoint modes in LST and nonlinear interaction terms in (8). The time-stepping procedure was performed using third-order Total Variation Diminishing (TVD) Runge-Kutta method (Gottlieb & Shu (1998)). To validate the WNLOP results with a fully nonlinear evolutions, we compare the results obtained by ILES using the same numerical framework. This scheme commonly adopts the numerical evaluation of spatial derivatives and time marching, which allows us to compare the WNLOP and ILES directly minimizing discrepancies arising from numerical discretization. To suppress the evolution of high wavenumber

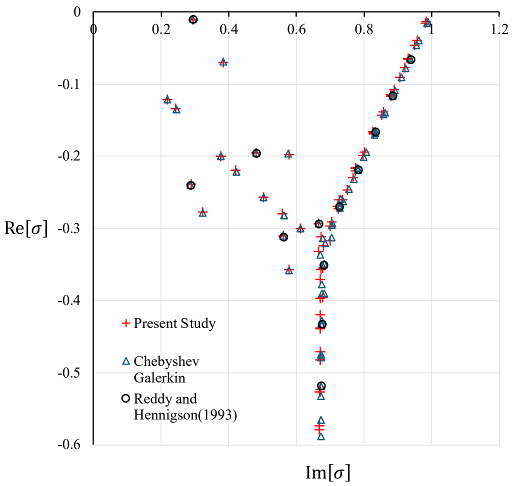

Figure 1: Distribution of eigenvalues at $M = 0.3, Re = 3000, k_x = 1, k_y = 0$. Reddy & Henningson (1993) calculates in 2D incompressible flow.

exceeding the effective wavenumber of compact difference scheme, we applied the 10-th order compact filtering method by Gaitonde & Visbal (2000) with $\alpha_f = 0.495$ to control the filtering strength. This method was also commonly applied to ILES and WNLOP for the evaluation of nonlinear term in (8).

The total number of grid point is 256 points clustered near the wall. To extend it to the three-dimensional ILES calculation, we considered the computational domain of $[0, 4\pi]$ for streamwise and $[0, 2\pi]$ for spanwise direction, which spans two wavelengths of the fundamental mode, $k_x = 1$, as a main target of present calculation and we will discuss it later. The numerical grid points for x, z are 1024 and 256, respectively. These assumptions of numerical grid points are sufficient to consider the higher harmonic waves to validate the theoretical limitation of the present study.

The flow field is set to the supercritical condition of plane-Poiseuille flow (pPF) field at $M = 0.3, Re = 3000, Pr = 0.72$. This flow condition is the same as the flow setting by Reddy & Henningson (1993); Hooper & Grimshaw (1996). Figure 1 shows the distribution of eigenvalues, along with the 2D incompressible eigenmodes from Reddy & Henningson (1993). Because we use compact finite difference method, the spurious modes exist due to its finite discretization properties, and we removed the modes which have most of their energy concentrated in the high-wavenumber components beyond the effective wavenumber. In the actual steps, we applied the compact filtering method and selected only those modes for which the relative error between the filtered and original vectors remained below 1%. Naturally, the choise of this threshold significantly influences the modes selection, and we compared the results obtained from Chebyshev-Collocation method using Shen's basis function (Shen (1994)) as a reference data (also shown in the same figure). We specifically adopt the leading 80 eigenmodes satisfying $\sigma_i > -0.66$. This selection corresponds to the principal 14 modes of the incompressible Orr-Sommerfeld equation, for which Reddy & Henningson (1993) demonstrates the convergence of LOP with a sufficient number of eigenmodes. These Orr-Sommerfeld modes are reproduced as the degenerate eigenmodes in the 3D compressible linearized N–S equations.

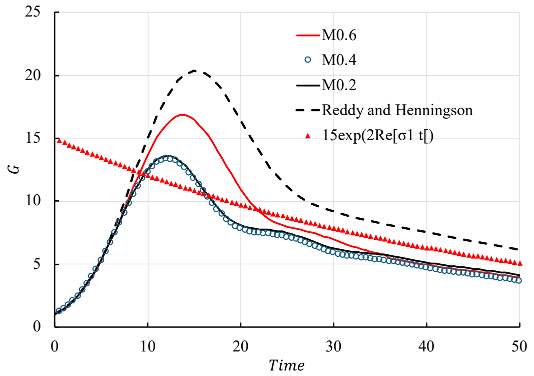

Figure 2: $G(t_f)$ for plane Poiseuille flow when $k_x = 1, k_y = 0$ and $Re = 3000$.

Results

Figure 2 shows the amplification of the disturbance field for the linear case where the second term in the RHS of (13) is omitted and the WNLOP reduces to LOP. In this figure, we plot the changes of amplification rate $G(t_f) := ||q'(t_f)||_a^2 / ||q'(0)||_a^2$. It is observed that the present result recovers the upward-convex functional shape for the disturbance amplification rate reported by previous studies (Reddy & Henningson (1993); Hooper & Grimshaw (1996)). We also confirmed that the slopes of amplification rate for longer evaluation time $t_f \geq 40.0$ are asymptotically consistent with the exponential growth $\exp(2\mathrm{Re}[\sigma_1]t)$, as discussed in Hooper & Grimshaw (1996). However, the present results slightly lower than those for incompressible flows presumably due to the difference in the norm definitions for compressible and incompressible flow field. Despite Hanifi *et al.* (1996) reporting that the amplification rates for compressible and incompressible disturbances coincide in the incompressible limit for Blasius boundary layer, the underestimation of the disturbance growth rate in plane Poiseuille flow suggests that acoustic disturbances play a critical role in internal flows.

Figure 3 compares the computational accuracy of the full-tensor calculation without contraction and TT decomposition at $M = 0.2$, focusing on the temporal evolution of the disturbance field initialized with uniform noise. It is observed that the relative error of the TT decomposition remains sufficiently small compared to the magnitude of the full-tensor calculation, thereby ensuring the numerical accuracy required to solve (13).

The characteristics of the optimization process of WNLOP are considered to be essential to understand the weakly nonlinear effect. Figure 4 shows the relation between the disturbance growth and gradient of the Lagrangian during the process. First, it is observed that the iterations for small amplitude δ_0 disturbance field show a good convergence during the optimization process (e.g., $\delta_0 = 0.0001, 0.0002$). Second, it is observed that the large initial disturbance amplitude shows a clear departure from smooth convergence by the gradient explosion of Lagrangian, the threshold for which appears to lie between 0.0007 and 0.0008 as the disturbance amplitude at the evaluation time. This gradient explosion vector is considered to be the amplification of disturbance field by exploiting positive Landau coefficients in the weakly nonlinear model, which destabilizes the optimization process itself (e.g., $\delta_0 = 0.0005$). Indeed, it is observed that these optimal solutions with a large gradient produced the rapid nonlinear growth immediately after the linear amplification of the disturbance field. The detailed evolution will be further discussed in the context of Fig.

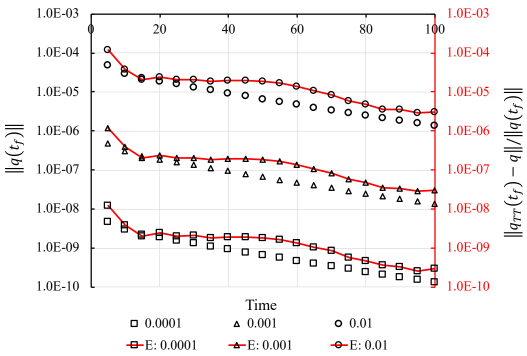

Figure 3: Time evolution of the disturbance norm initialized with uniform random noise, showing the full-tensor calculation $||q||$ and the corresponding relative error of the approach based on TT decomposition (using the leading 20 eigenmodes).

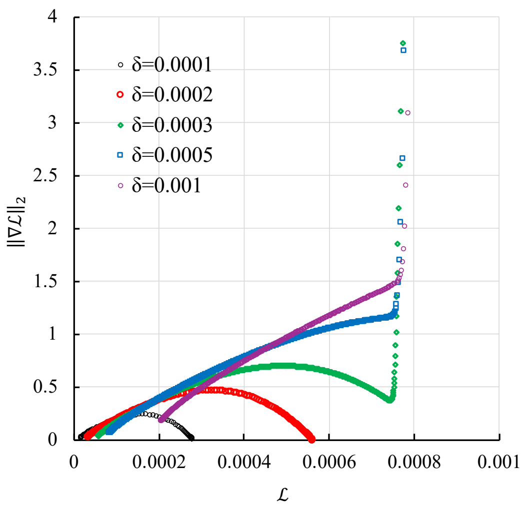

Figure 4: The history in optimization process at $t_f = 20.0$ and each initial disturbance magnitude with respect to the disturbance magnitude at the evaluation time and the gradient of the Lagrangian.

6. The physical existence of these amplification mechanism cannot be easily ruled out within the current framework, but it may be stem from numerical artifacts inherent in the weakly nonlinear model because the reproduction using ILES has not yet been achieved. More rigorous discussions are required in this point.

Figure 5 shows the time-evolution of disturbance amplitude. In this figure, we plotted the time-evolution of disturbance magnitude with different initial disturbance amplitudes, where the disturbance growth properties deviate slightly from the linear-like behavior observed at $\delta_0 = 0.0001$. In this figure, we selected the case of $\delta_0 = 0.0003$, where the disturbance amplitude at t_f is 0.000746 and gradient amplitude 0.371 just before the gradient explosion from Fig. 4. Meanwhile, we selected the case of $\delta_0 = 0.0005$, where the disturbance amplitude at t_f is 0.000762 and 0.000780 and a gradient amplitude 1.28 and 3.67 as just before and after the gradient explosion, respectively. In these large-amplitude cases, the case at $\delta_0 = 0.0005$ after the gradient explosion shows that the second peak of disturbance evolution after the initial growth phase. Figure 6 shows a comparison between the temporal evolution

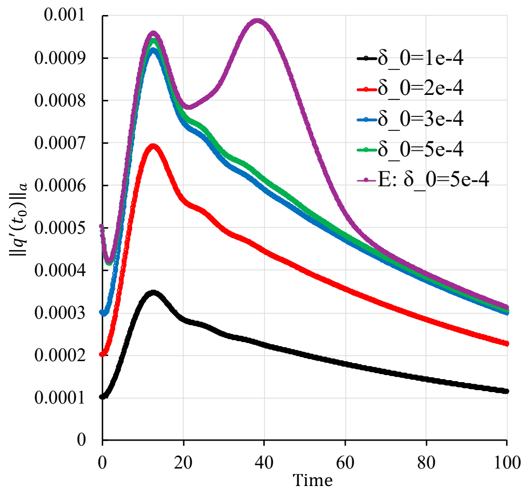

Figure 5: Time evolution of disturbance amplitude of WNLOP with different initial disturbance magnitudes at $t_f = 20.0$. "E" denotes the WNLOP after the occurrence of gradient explosion.

of disturbance field in weakly nonlinear model and ILES at these two cases. For the case $\delta_0 = 0.0003$, we observed that excellent agreement between the weakly nonlinear model and ILES except for a slight underestimation of amplitudes during its time-evolution. Because this amplitude underestimation is almost identical during its time-evolution, it is considered that the deviation is originated from the numerical discrepancies between the ILES and WNLOP, rather than the intrinsic nonlinear effect. However, the time-evolution of disturbance growth after the gradient explosion shows a clear deviation especially for the second peak, even though it achieved a high degree of agreement between these models until $t = 20.0$. Thus, this evolution of secondary peak is considered to be numerical artifacts inside the weakly nonlinear model, which is difficult to reproduce in the ILES. This observation confirms the high reliability in its accuracy of prediction in weakly nonlinear model at sufficiently small amplitude, but it also suggests that the limitation of current model to track larger amplitude disturbance growth.

Figure 7 shows the time-evolution of disturbance field in each wavenumber component at $\delta_0 = 0.0003$ of fundamental wave k, mean component 0, and harmonic waves $2k, 3k, 4k, 5k$, from the calculation of ILES. Each wavenumber component is obtained by the discrete Fourier analysis and $F[\cdot]$ denotes the norm defined in (20). In this figure, we observed that the amplitude of high-harmonic waves of $2k, 3k$ increases with the time-evolution, while $4k, 5k$ remain at low levels. At $t = 10.0$, the order of amplitude at each $k, 2k, 3k$ are $O(10^{-3}).O(10^{-6}), O(10^{-8})$, respectively, which almost satisfies the assumptions of scale separations in weakly nonlinear analysis. The evolution of higher harmonic waves are obtained as predicted by theory, which is in agreement with the amplitude expansion method. In the order of $O(\varepsilon^2)$, it is observed that the effect of mean flow distortion and double-harmonic waves are of the same order of magnitude. This point indicates that the present WNLOP considers both effects of mean-flow distortion and double-harmonic waves as the weakly nonlinear mechanism of optimal perturbation, which is a significant advancement beyond Pralits *et al.* (2015).

Differences in the functional shapes in the reconstructed initial WNLOP are presented in Fig. 8. From this figure, it is

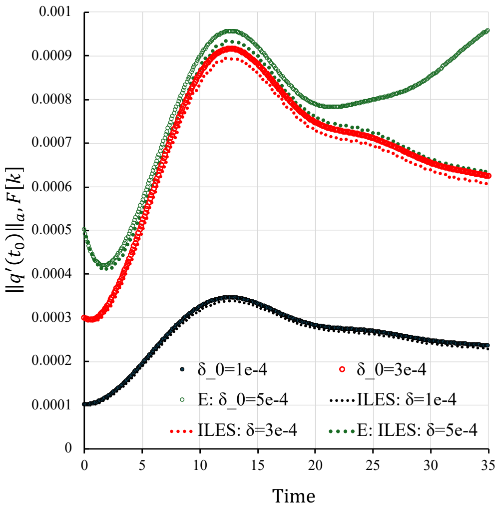

Figure 6: Time evolution of disturbance amplitude of WNLOP with different initial disturbance magnitudes at $t_f = 20.0$.

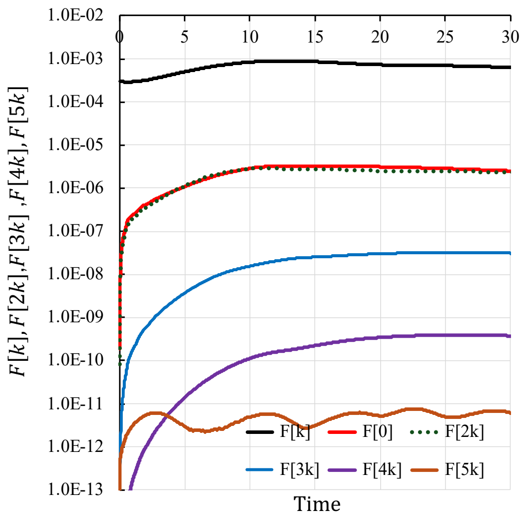

Figure 7: Time-history of amplitude of each wavenumber components during the evolution of WNLOP at $t_f = 20.0, \delta_0 = 0.0003$.

observed that for the small initial disturbance amplitude, the spanwise velocity distribution is almost uniformly zero. This is consistent with the two-dimensional incompressible flow settings assumed in previous studies (Reddy & Henningson (1993); Hooper & Grimshaw (1996)). However, as the initial disturbance amplitude increases, the relative significance of the streamwise velocity u_x decreases while retaining a similar spatial distribution, whereas the magnitude of the spanwise velocity increases. The intensity of this spanwise velocity distribution was slowly decreased during the initial time-evolution corresponding to the initial decrease of disturbance magnitude in Fig. 6. For the optimal perturbation which produces the spurious secondary peak at $\delta_0 = 0.0005$, we observed that the changes of functional shape are negligible before and after the gradient explosion. This point suggests that the generation of spurious secondary peak is originated from the specific combination of eigenmodes which utilizes the positive Landau coefficient, and small changes in functional shape causes this amplification to increase.

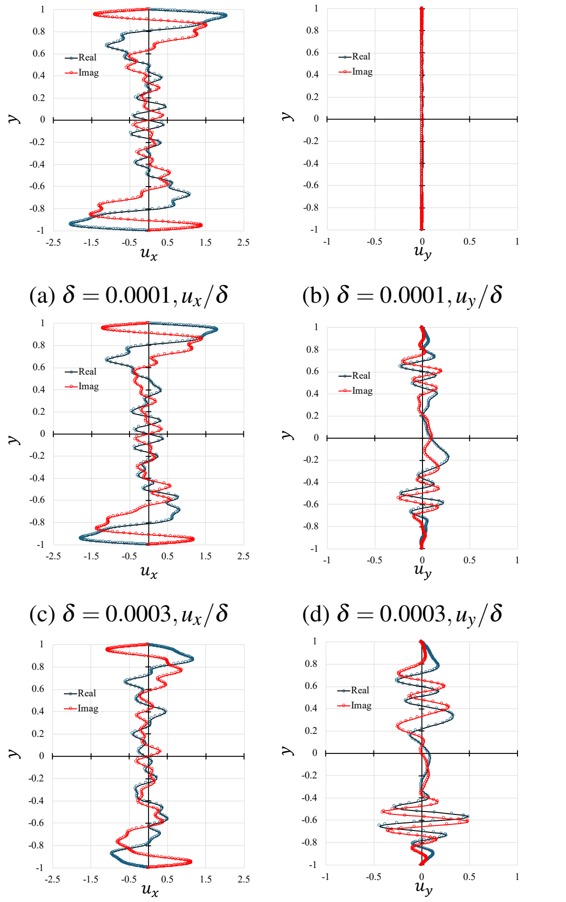

(a) $\delta = 0.0001, u_x/\delta$ (b) $\delta = 0.0001, u_y/\delta$

(c) $\delta = 0.0003, u_x/\delta$ (d) $\delta = 0.0003, u_y/\delta$

(e) $\delta = 0.0005 u_x/\delta$ (f) $\delta = 0.0005, u_y/\delta$

Figure 8: Spatial distribution of WNLOP at $t_f = 20$ and different initial disturbance amplitude (Real part: black line and Imaginary part: red line). The values are normalized by the initial disturbance magnitude.

Conclusion

In this study, we considered the weakly nonlinear optimal perturbation theory based on the coupled amplitude equations. Based on the several assumptions regarding the nonlinear interaction terms and the normalization of disturbances, the current framework successfully captures the effect of mean flow distortion and double-harmonic waves on the evolution of optimal perturbation under small-amplitude initial conditions in the small-amplitude regime. The present analysis shows a good agreement between the prediction by WNLOP and ILES, while it shows a clear deviation originated from the spurious second peak in the later stages of time-evolution.

REFERENCES

Butler, Kathryn M & Farrell, Brian F 1994 Nonlinear equilibration of two-dimensional optimal perturbations in viscous shear flow. *Physics of Fluids* **6** (6), 2011–2020.

Cherubini, Stefania, De Palma, Pietro, Robinet, J-Ch & Bottaro, Alessandro 2010 Rapid path to transition via nonlinear localized optimal perturbations in a boundary-layer flow. *Physical Review E* **82** (6), 066302.

Drazin, Philip G & Reid, William Hill 2004 *Hydrodynamic stability*. Cambridge university press.

Ducimetière, Yves-Marie & Gallaire, François 2025 Non-modal amplitude equations. *Physical Review E* **112** (1), 015101.

Fujimura, K 1989 The equivalence between two perturbation methods in weakly nonlinear stability theory for parallel shear flows. *Proceedings of the Royal Society of London. A. Mathematical and Physical Sciences* **424** (1867), 373–392.

Gaitonde, Datta V & Visbal, Miguel R 2000 Padé-type higher-order boundary filters for the Navier–Stokes equations. *AIAA journal* **38** (11), 2103–2112.

Gottlieb, Sigal & Shu, Chi-Wang 1998 Total variation diminishing Runge-Kutta schemes. *Mathematics of computation* **67** (221), 73–85.

Hanifi, Ardeshir, Schmid, Peter J & Henningson, Dan S 1996 Transient growth in compressible boundary layer flow. *Physics of Fluids* **8** (3), 826–837.

Hooper, AP & Grimshaw, R 1996 Two-dimensional disturbance growth of linearly stable viscous shear flows. *Physics of Fluids* **8** (6), 1424–1432.

Kerswell, RR 2018 Nonlinear nonmodal stability theory. *Annual Review of Fluid Mechanics* **50**, 319–345.

Landau, Lev Davidovich & Lifshitz, Evgenii Mikhailovich 2013 *Fluid Mechanics: Landau and Lifshitz: Course of Theoretical Physics, Volume 6*, , vol. 6. Elsevier.

Lele, Sanjiva K 1992 Compact finite difference schemes with spectral-like resolution. *Journal of computational physics* **103** (1), 16–42.

Mack, Leslie M 1984 Boundary-layer linear stability theory. *Agard rep* **709**.

Oseledets, Ivan V 2011 Tensor-train decomposition. *SIAM Journal on Scientific Computing* **33** (5), 2295–2317.

Pralits, Jan O, Bottaro, Alessandro & Cherubini, Stefania 2015 Weakly nonlinear optimal perturbations. *Journal of Fluid Mechanics* **785**, 135–151.

Pringle, Chris CT & Kerswell, Rich R 2010 Using nonlinear transient growth to construct the minimal seed for shear flow turbulence. *Physical review letters* **105** (15), 154502.

Reddy, Satish C & Henningson, Dan S 1993 Energy growth in viscous channel flows. *Journal of Fluid Mechanics* **252**, 209–238.

Rigas, Georgios, Sipp, Denis & Colonius, Tim 2021 Nonlinear input/output analysis: application to boundary layer transition. *Journal of Fluid Mechanics* **911**, A15.

Shen, Jie 1994 Efficient spectral-galerkin method i. direct solvers of second-and fourth-order equations using legendre polynomials. *SIAM Journal on Scientific Computing* **15** (6), 1489–1505.

Trefethen, Lloyd N, Trefethen, Anne E, Reddy, Satish C & Driscoll, Tobin A 1993 Hydrodynamic stability without eigenvalues. *Science* **261** (5121), 578–584.

Watson, J 1960 On the non-linear mechanics of wave disturbances in stable and unstable parallel flows part 2. the development of a solution for plane poiseuille flow and for plane couette flow. *Journal of Fluid Mechanics* **9** (3), 371–389.